

Molecular BioSystems

Accepted Manuscript



This is an *Accepted Manuscript*, which has been through the Royal Society of Chemistry peer review process and has been accepted for publication.

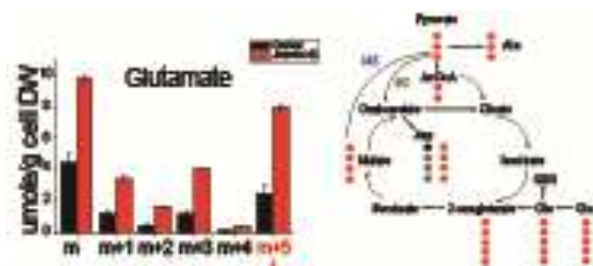
Accepted Manuscripts are published online shortly after acceptance, before technical editing, formatting and proof reading. Using this free service, authors can make their results available to the community, in citable form, before we publish the edited article. We will replace this *Accepted Manuscript* with the edited and formatted *Advance Article* as soon as it is available.

You can find more information about *Accepted Manuscripts* in the [Information for Authors](#).

Please note that technical editing may introduce minor changes to the text and/or graphics, which may alter content. The journal's standard [Terms & Conditions](#) and the [Ethical guidelines](#) still apply. In no event shall the Royal Society of Chemistry be held responsible for any errors or omissions in this *Accepted Manuscript* or any consequences arising from the use of any information it contains.



www.rsc.org/molecularbiosystems



Jhdm1b knock down cells enhanced glutaminolysis to maintain Krebs cycle by upregulating RIP3 expression.

ARTICLE

Systematic study of the cellular metabolic regulation of Jhdm1b in tumor cells

Cite this: DOI: 10.1039/x0xx00000x

Xi Yu¹, Jiayu Wang², Jihui Wu^{1*}, Yunyu Shi^{1*}

¹From Hefei National Laboratory for Physical Sciences at Microscale and School of Life Sciences, University of Science and Technology of China, Hefei, Anhui, 230026, China.

Received 00th January 2012,
Accepted 00th January 2012

DOI: 10.1039/x0xx00000x

www.rsc.org/

Metabolic alterations have been observed in cancer for almost a century. More attention now is directed toward the mechanisms underlying these changes. Jhdm1b (Fbx110/Kdm2b), an H3K4/K36 histone demethylase overexpressed in various types of cancer, has been reported to regulate cell proliferation and senescence in HeLa cells. In this work, we used ¹³C stable isotope resolved metabolomics to investigate cellular metabolites, including intermediates of glycolysis, pentose phosphate pathway, and Krebs cycle. The difference in the concentration of cellular metabolites of wild-type and Jhdm1b knockdown HeLa cells indicates that Jhdm1b is a positive regulator of glycolysis, glutaminolysis, and pyrimidine synthesis in HeLa cells. Double knockdown experiments showed that Receptor-interacting serine/threonine-protein kinase 3 (RIP3), a protein kinase of the cell, is critical to the metabolic shifts induced by Jhdm1b depletion.

INTRODUCTION

Metabolic alterations, such as Warburg effect¹ and glutaminolysis², are common features of primary and metastatic human tumors. To satisfy the requirements of energy production and biomass synthesis for rapid proliferation, tumor cells tend to choose a faster but less efficient way to utilize nutrients, such as glucose and glutamine. They usually increase the uptake of glucose and glycolysis to secrete lactate even under aerobic conditions. Tumor cells need to upregulate glutaminolysis and anaplerotic reactions to sustain the Krebs cycle activity and to provide more precursors for the synthesis of biomass, such as amino acids, fatty acids, and nucleotides³. Furthermore, numerous tumor suppressors and oncogenes regulate the metabolic pathways directly or indirectly in mammalian cells. p53⁴ and C-MYC⁵ are the two most common tumor suppressors related to metabolic regulation.

Recent study⁶ indicates that the Krebs cycle intermediates can be shaped by the epigenetic landscape of chromatin by regulating DNA and histone modification. In mammalian cells, the histone lysine methylation state is related with histone lysine methyltransferases (KMTs) and demethylases (KDMs). As a KDM, JMJD5 has been demonstrated to interact directly with pyruvate kinase muscle isozyme2 (PKM2) to modulate metabolic flux in cancer cells⁷. These findings suggest that KMTs and KDMs may be important in cell metabolism.

Jhdm1b/Kdm2b/Fbx110, a member of Jhdm (JmjC-domain-containing histone demethylase) family, is an H3K4/K36 histone demethylase. Jhdm1b is overexpressed in various types of cancer⁸.

INK4b-ARF-INK4a locus encodes three tumor-suppressor proteins, namely, p15^{INK4b}, p14^{ARF}, and p16^{INK4a}, and is critical to both cellular senescence and tumorigenesis. This locus constitutes an important barrier for tumor growth. Jhdm1b targets the p15^{INK4b} locus and regulates its expression, whereas Jhdm1b knockdown in primary mouse embryo fibroblasts (MEFs) inhibits cell proliferation and induces cellular senescence⁹.

Recently, some evidence has shown that Jhdm1b plays an important role in regulating cell metabolism. Microarray experiments revealed that about 50% of the Jhdm1b target genes, such as RIP3 and cellular retinoic acid-binding protein II (Crabp2), are linked to cell metabolism¹⁰. Crabp2 associates with retinoic acid (RA) and enhances the transcriptional activity of RA receptor. RIP3 interacts with RIP1 to form a complex mediating necrotises. Moreover, RIP3 regulates several metabolic enzymes, such as glycogen phosphorylase (PYGL), glutamate-ammonia ligase (GLUL) and glutamate dehydrogenase 1 (GLUD1) that enhance the metabolism-associated ROS production.

Although previous work indicates that Jhdm1b may be relevant to metabolic alterations in cancer cells, a systematic investigation on the metabolic regulation of Jhdm1b in tumor cells remains lacking. In this work, we used U-¹³C glucose/glutamine and 1,2-¹³C glucose as carbon sources to study the differences in carbon central metabolism between Jhdm1b knockdown and wild-type HeLa cells based on two complementary approaches: gas chromatography–mass spectrometry (GC–MS) and nuclear magnetic resonance (NMR). GC-MS can precisely determine the metabolite concentrations, but it is unsuitable for a wide range of metabolites. On the other hand,

NMR can quantify more metabolites and provide their structural information. Our results reveal that Jhdm1b is an RIP3-dependent regulator of cancer metabolism and may aid in the function exploration of histone demethylases in tumor cellular metabolic regulation which can potentially provide new ideas for cancer therapy.

RESULTS

Knockdown of Jhdm1b in HeLa cells inhibits cell proliferation.

We knocked down Jhdm1b in HeLa cells through RNA interference¹¹. qRT-PCR experiments were conducted to verify the knockdown efficiency (Figure 1A). The expression level of Jhdm1b after knockdown was about 30% of that in wild-type cells. The growth curves of wild-type and Jhdm1b knockdown cells during six days (Figure 1B) showed that the cell proliferation was inhibited in Jhdm1b knockdown cells.

Glycolysis is suppressed in Jhdm1b knockdown cells.

We determined the metabolic differences between wild-type and Jhdm1b knockdown HeLa cells cultured with medium containing uniformly labeled [U-¹³C]-glucose. [1,2,3-¹³C]-lactate and Ala should be produced by [U-¹³C]-glucose through glycolysis. We observed that Jhdm1b knockdown reduced the secreted m+3 isotopologue (the molecules that differ only in their isotopic composition) of lactate in media after 24 h (Figure S1A), suggesting the anaerobic respiration is decreased. The concentration of m+3 isotopologue of Ala also decreased after Jhdm1b depletion (Figure S1B), which may indicate a lower rate of the aerobic respiration in the Jhdm1b knockdown cell line because Ala comes from pyruvate. The NMR data of ¹³C isotopologues of intracellular lactate and Ala were consistent with the GC-MS analysis. The satellite peaks of lactate and Ala in TOCSY spectra indicated that most C2 and C3 carbons of these two metabolites were ¹³C-labeled (Figure S3A), whereas in Jhdm1b knockdown cells a lower degree of ¹³C enrichment for lactate and Ala was observed (Figure S1A, 2C), which means that the proportion of unlabeled Ala and lactate is higher in Jhdm1b knockdown cells. In tumor cells, the fraction of unlabeled Ala and lactate may reflect the contributions from other metabolic pathways such as protein turnover or glutaminolysis. Therefore, it is possible that these pathways are upregulated in Jhdm1b knockdown cells.

Furthermore, using qRT-PCR, we measured the gene expression level of lactate dehydrogenase (LDH), which catalyzes the conversion of L-lactate and NAD to pyruvate and NADH in the final step of glycolysis. The downregulation of LDH expression (Figure 4A) indicates that the anaerobic respiration was inhibited in Jhdm1b knockdown cells. According to Warburg effect, glycolytic flux is dominant even under aerobic conditions in cancer cells. Thus, LDH downregulation may result in reduced pyruvate production.

Krebs cycle activity is sustained in Jhdm1b knockdown cells.

Using [U-¹³C]-glucose as the tracer, GC-MS data showed that the levels of most of the Krebs cycle intermediates were sustained in Jhdm1b knockdown cells. [1,2-¹³C]-Acetyl-CoA from [U-¹³C]-glucose enters Krebs cycle to form intermediates with two ¹³C atoms. As shown in Figure S1C, the constant quantities of m+2 succinate, malate and elevated m+2 citrate suggest that Krebs cycle activity was sustained when Jhdm1b was knocked down. These results are consistent with the NMR data in which the intensity of doublet of C3 carbon did not decrease for malate (Figure S3A).

The decreased glycolysis flux resulted in the production of less pyruvate in Jhdm1b knockdown cells, but the concentrations of the Krebs cycle intermediates in these cells remained at a similar or slightly higher level. This contradiction may be explained by the activation of Pyruvate dehydrogenase (PDH), pyruvate carboxylation (PC) pathway and glutaminolysis. These three pathways were determined to explore whether they were enhanced to maintain the Krebs cycle activity.

Oxidative decarboxylation of pyruvate is known to link glycolysis and the Krebs cycle. PDH is a mitochondrial multienzyme complex that catalyzes the conversion of pyruvate to acetyl coenzyme A (AcCoA). We measured the enzyme activity and expression level of PDH. Our results indicated that PDH expression level was slightly reduced in Jhdm1b knockdown cells (Figure 4A), but its activity increased by more than fourfold (Figure 4B). Enhanced PDH activity should increase AcCoA production and cause more m+2 intermediates to enter the Krebs cycle when Jhdm1b is knocked down.

The increased m+5 citrate is attributed to the enhancement of PC pathway because the m+5 citrate is synthesized by m+2 AcCoA plus m+3 oxaloacetate from pyruvate carboxylation¹². since the m+3 oxaloacetate cannot be detected directly, its products, m+3 malate and succinate, were monitored using GC-MS in Jhdm1b knockdown cells. Our results indicated that their cellular levels remained unchanged upon the depletion of Jhdm1b (Figure S1C). Considering pyruvate production was inhibited as mentioned above, the PC pathway activity must be upregulated to maintain the concentration of m+3 malate and succinate.

To study whether glutaminolysis was activated in Jhdm1b knockdown cells, we used [U-¹³C]-Gln as the tracer to determine the fate of glutamine. The cellular m+5 Glu converted from m+5 Gln by glutaminase obviously increased in Jhdm1b knockdown cells (Figure S2A). [U-¹³C]-Gln forms [U-¹³C]- α -ketoglutarate by deamination to enter the Krebs cycle and then produces m+4 intermediates such as malate and fumarate. The increase in m+4 malate, fumarate, and citrate suggests that Gln entry into the Krebs cycle was activated by Jhdm1b knockdown (Figure S2C). The more active glutaminolysis in Jhdm1b knockdown cells enhanced de novo glutathione (GSH) synthesis. GSH is biosynthesized in the body form from Cys, Glu and Gly. Using [U-¹³C]-glucose as the tracer, the Glu residue of GSH was labeled and the labeling extents were stronger in Jhdm1b knockdown cells than in wild-type (Figure S3B). Cys, the rate-limiting substrate of GSH synthesis, was excessive in the media.

Thus, the labeled Glu incorporation could reflect GSH synthesis activity correctly.

There is another possible pathway to regulate the Krebs cycle. The malic enzyme (ME) catalyzes the oxidative decarboxylation of malate to pyruvate¹³(Figure S2B). If ME is activated, the increased pyruvate will produce more AcCoA to enhance the Krebs cycle. Pyruvate is the precursor of Ala, so the low concentration of m+3 Ala suggests that neither wild-type nor Jhdm1b knockdown cells preferred to produce glutamine-derived pyruvate when glucose is abundant. Concentrations of m+3/m+5 citrate and m+3 Asp, which were derived from ME-PC pathway, were very low in both cells, also suggesting ME is inactivated.

Nucleotide biosynthesis is reduced in Jhdm1b knockdown cells.

Asp is a direct precursor of pyrimidine and purine providing a part of the carbon skeleton and some nitrogen atoms for pyrimidine biosynthesis. However, oxaloacetate, the precursor of Asp, exhibits no detectable signals in GC–MS or NMR experiment. On the other hand, Asp is a direct precursor of 5'-UXP, and both of them show similar labeled pattern of uracil ring in TOCSY spectrum³. Therefore TOCSY experiment was employed to detect the cross peaks of 5'-UXP and reveal the structure information of Asp. All satellite peaks of 5'-UXP C5C6 observed in the TOCSY spectra (Figure S3 suggested that [¹³C-1,2,3]-Asp and [¹³C-1,2]-Asp both existed in wild-type and knockdown HeLa cells. [¹³C-1,2,3]-Asp can only be synthesized from [¹³C-1,2,3]-malate via pyruvate carboxylation, whereas [¹³C-1,2]-Asp comes from normal Krebs cycle. Therefore, these two pathways are both activated in wild-type and Jhdm1b knockdown cells.

The abundance of all 5'-UXP C5C6 isotopologues decreased in Jhdm1b knockdown cells, consistent with the GC–MS data of Asp. This finding suggests that the pyrimidine synthesis was downregulated when Jhdm1b was knocked down. The weak signals of other cross peaks of 5'-AXP and -UXP in HSQC spectra of Jhdm1b knockdown cells indicates a low rate of nucleotide synthesis (Figure S3).

In addition, the decrease in the expression of Asp carbamyl transferase (ACT), which catalyzes the reaction of pyrimidine synthesis, may also result in a decrease in nucleotide synthesis in Jhdm1b knockdown cells (Figure 4A).

Phosphate pentose pathway is not influenced by Jhdm1b knockdown.

Previous study¹⁴ showed that the expression of several anti-oxidant genes is regulated by Jhdm1b. To learn whether Jhdm1b can affect the flux ratio distribution of phosphate pentose pathway in human cancer cells, DMEM medium containing [1,2-¹³C]-glucose was used to estimate the activity of phosphate pentose pathway¹⁵. Regular glycolysis produces m+2 isotopologue of lactate in [1,2-¹³C]-glucose medium. The m+1 isotopologue of Ala and lactate can only be synthesized by pyruvate via the phosphate pentose (PP)

pathway. Thus, the ratio of these two isotopologues can reflect the activity of the PP pathway.

Our GC–MS results showed that the ratio of m+1 to m+2 isotopologues of lactate exhibited no obvious difference between wild-type and Jhdm1b knockdown cells (Figure 2B). In addition, the ratio of [2,3-¹³C] lactate to [3-¹³C] lactate reflects the flux ratio of glycolysis to PP pathway¹⁵. We therefore determined the ratio of peak intensities of [3-¹³C] lactate to [2,3-¹³C] lactate in HSQC spectra and observed only a slight difference between them (Figure 2A). Together our GC-MS and NMR results suggest that Jhdm1b did not change the proportion of glycolysis to PP pathway to regulate redox homeostasis.

Jhdm1b knockdown activates RIP3 expression but does not affect programmed necrosis.

RIP3 is a serine/threonine-protein kinase. It directly interacts with and activates several metabolism-related enzymes. The expression level of RIP3 was elevated in Jhdm1b knockdown cells (Figure 3), consistent with previous studies that Jhdm1b targets to the promoter of RIP3 and significantly reduces the level of H3K4me3¹⁰. RIP1, an important regulator of programmed necrosis, did not significantly change at the mRNA level (Figure 3A).

Expression and activity of RIP3-relevant metabolic enzymes change in Jhdm1b knockdown cells.

The activities and expression levels of some important metabolic enzymes were measured to estimate the influence of Jhdm1b depletion on cell metabolism. According to the previous reports¹⁰, Jhdm1b downregulates the expression of RIP3, which activates the metabolic enzymes PYGL, GLUL, and GLUD1. RT-PCR data showed that the expression levels of PYGL and GLUD1 were slightly elevated in Jhdm1b knockdown cells and that of GLUL remained unchanged (Figure 4A). Their enzyme activities all increased in Jhdm1b knockdown cells (Figure 4B).

RIP3 knockdown partly converts metabolic changes in Jhdm1b knockdown cells.

To learn the function of RIP3 in metabolic shifts induced by Jhdm1b depletion, we generated Jhdm1b/RIP3 double knockdown cells and used GC–MS to investigate their carbon central metabolism change (Figure S4A). Using [U-¹³C] Gln as the tracer, the lower m+5 Glu concentration observed in our experiment suggests that glutaminolysis activity was downregulated when RIP3 was knocked down (Figure S4B). The m+4 isotopologues of the Krebs cycle intermediates, such as fumarate and citrate, decreased in double knockdown against Jhdm1b knockdown cells (Figure S4C). In addition, RT-PCR data indicate that the expression levels and activities of GLUL, GLUD1, and PYGL all decreased in Jhdm1b/RIP3 knockdown (Figures 5A, 5B). Together these results suggest that enhanced glutaminolysis was induced by RIP3 upregulation in Jhdm1b knockdown cells.

However, Asp concentration remained low in Jhdm1b/RIP3 double knockdown cells, and the expression levels of ACT in single and double knockdown cells were similar. These results indicate a possibility that RIP3 alone is not responsible for the decreased pyrimidine synthesis in Jhdm1b knockdown cells.

DISCUSSION

Jhdm1b promotes cell proliferation accompanied by activation of energy metabolism and biomass synthesis of tumor cells.

In tumor cells, energy metabolism and biomass synthesis are activated to meet the requirement of rapid growth and proliferation. Jhdm1b is a member of the JmjC domain-containing histone lysine demethylase family (JmjC class KDM). Jhdm1b targets the p15^{INK4b} locus and recruits PRC1 to regulate the expression of INK4b-ARF-INK4a locus, which is important for cell senescence and tumorigenesis¹⁶. Jhdm1b overexpression significantly increases the growth rate in MEFs and increase the expression of some metabolism-related genes¹⁷. Its overexpression has also been reported to promote tumor cell proliferation and inhibit cell senescence⁹. However, there are so far no systematic studies on the effects of this KDM on the metabolic network in cancer cells.

In this research, a sharp decline was observed in the growth rate of Jhdm1b knockdown cells (Figure 1). GC-MS data showed that the concentrations of m+3 lactate and Ala in these cells were reduced (Figure S1), while NMR analysis exhibited that the cross-peaks of lactate and Ala significantly decreased in intensity (Figure S3A). These results indicated that glycolysis was downregulated and biomass synthesis was less active in Jhdm1b knockdown cells. Moreover, decreased Asp and 5'-AXP/UXP suggests that pyrimidine synthesis is suppressed in Jhdm1b knockdown cells (Figure S3A), consistent with the downregulation of the biosynthetic pathways. RT-PCR data showed that ACT, the key metabolic enzyme in pyrimidine synthesis pathway, was downregulated when Jhdm1b was knocked down.

In summary, our results indicate that Jhdm1b is a positive growth regulator of tumor cells. Jhdm1b activates the expression of carbon central metabolic enzymes to provide energy and materials for the rapid growth of tumor cells. These findings indicate that Jhdm1b may become a potential target for the design or screening of the anticancer drugs.

PDH is activated by Jhdm1b knockdown

In this study, for the first time we demonstrate that Jhdm1b knockdown could significantly increase PDH activity. PDH is central to the bridging of glycolytic metabolism in the cytosol with the Krebs cycle and oxidative phosphorylation in the mitochondria by irreversibly converting pyruvate and NAD⁺ into acetyl-CoA, NADH, and carbon dioxide. To maintain cellular energy homeostasis and to supply the necessary carbon to the biosynthetic pathways intersecting the Krebs cycle, the activity of PDH must be fine-tuned. The PDH deficiency defined by reduced PDH activity is

an important phenomenon in patient cells related to numerous diseases^{18, 19}.

It has been well known that the regulation of PDH activity is achieved by phosphorylation and dephosphorylation performed by the pyruvate dehydrogenase kinases and the pyruvate dehydrogenase phosphatases²⁰. Recently, JMJD5, a Jumonji C domain-containing dioxygenase which is involved in lysine demethylation and hydroxylation, was proved to interact with pyruvate kinase muscle isozyme (PKM)2 directly and reduce glucose uptake and lactate secretion in cancer cells⁷. Similarly, Jhdm1b is also a JMJC domain-containing lysine demethylase. Our data indicated that Jhdm1b knockdown cells maintained the Krebs cycle activity by activating PDH. Whether Jhdm1b interacts with PDH directly and what is the molecular mechanism for PDH activity regulation needs more research.

Jhdm1b is an RIP3-dependent regulator of cancer metabolism.

Jhdm1b is a histone demethylase which preferentially demethylates trimethylated H3 Lys-4 and dimethylated H3 Lys-36 residues. Jhdm1b overexpression directly inhibits the expression of two metabolic enzymes, namely, RIP3 and Crabp2. CHIP assay showed that Jhdm1b interacts with their promoter regions and decreases H3K4 trimethylation levels in MEFs¹⁰. RIP3 complex was found to interact directly with the metabolic enzymes PYGL, GLUL, and GLUD1 to increase glucose and glutamine consumption²¹.

Our data showed that RIP3 expression was elevated in Jhdm1b knockdown HeLa cells (Figure 3). Our RT-PCR experiments showed that the expression levels of GLUL and GLUD1 were slightly elevated in Jhdm1b knockdown cells (Figure 4A). Their enzyme activity increased in Jhdm1b knockdown (Figure 4B) but decreased in RIP3/Jhdm1b double knockdown cells (Figure 5). This result suggests that Jhdm1b regulates RIP3 expression to activate GLUL and GLUD1, consistent with the earlier report²¹. GLUL catalyzes the condensation of glutamate and ammonia to form glutamine, and GLUD1 catalyzes the deamination of glutamine to α -ketoglutarate. Their activation results in increased glutamine-source intermediates of the Krebs cycle. Using [U-¹³C]-Gln as the tracer for SIRM analysis, m+4 fumarate, citrate, and malate all increased in Jhdm1b knockdown cells, suggesting that glutamine entry into the Krebs cycle was activated, which is consistent with the metabolic shifts induced by RIP3 activation. Furthermore, these intermediates declined in Jhdm1b/RIP3 knockdown cells. These data indicate that RIP3 plays a critic role in the metabolism regulation of Jhdm1b knockdown. GSH is the major endogenous antioxidant synthesized from Cys, Gln and Gly. Our data show that Jhdm1b knockdown not only enhanced Krebs cycle activity through glutaminolysis activation, but also activated de novo GSH biosynthesis (Figure S3B) to remove the oxidative metabolism product, ROS.

Despite the implication that histone methyl transferases and demethylases may act as energy sensors and serve an important function in the cellular metabolic pathway regulation, systematic research on the metabolic regulation of KTM and KDM remains

lacking. We systematically studied the function of Jhdm1b in the regulation of cellular metabolism in tumor cells. Our results indicate that Jhdm1b is a positive growth regulator of tumor cells. Jhdm1b activates the expression of carbon central metabolic enzymes to provide energy and biomass for the rapid growth of tumor cells. RIP3 is critical to metabolic regulation induced by Jhdm1b. We are also the first to report that Jhdm1b is relevant to the activity of PDH. Our data indicate that Jhdm1b may become a potential target for therapy against cancer and other diseases.

EXPERIMENTAL PROCEDURES

Cells, medium and isotopes

HeLa cell line were cultured in glucose and pyruvate-free Dulbecco's Modified Eagle's Medium (DMEM) (Gibco), supplemented with 100 IU/ml penicillin, 10 µg/ml streptomycin (Life Technologies) in the presence of 10% dialyzed FCS (Life Technologies) and 5mM glucose. The cells were cultured in the atmosphere at 5% CO₂, 37°C at an initial cell density of 2.5 × 10⁴ cells/dish. The media were changed every 48 h.

[U-¹³C]-glucose (99% ¹³C, Sigma-Aldrich), [1,2-¹³C]-glucose (99% ¹³C, Sigma-Aldrich) and [U-¹³C]-glutamine (99% ¹³C, Sigma-Aldrich) were purchased. Before ¹³C labeling, the cells were cultured in only 0.5% bovine serum albumin (BSA) to partially synchronize the culture for 24 h. For ¹³C labeled experiment, cells were cultured in normal medium for 24 h, then 1 × 10⁷ HeLa cells were plated in 10cm plates, washed with PBS twice and then media was replaced with glucose-free DMEM containing 5 mM [U-¹³C]/[1,2-¹³C]-glucose (or Gln-free DMEM containing 2mM [U-¹³C]-glutamine), 10% dialyzed FCS, 100 IU/ml penicillin and 10 µg/ml streptomycin ²². After 24 h, cells were harvested for metabolites extraction. The growth rates of cells were measured by direct counting on a hemocytometer using 0.4% Trypan Blue.

RNA interference

Lentiviruses containing the TRC shRNA (TRCN0000AAO40G5 for Jhdm1b, NM_006871.3 for RIP3) were produced in 293T packaging cells as the invitrogen user Manual. As a negative control, we used siCONTROL non-targeting siRNA.

Lipofectamine 2000 (invitrogen) was used as a transfection reagent. Knockdown efficiency was tested by RT-PCR or western blot.

The sequences used to check knockdown efficiency:

For Jhdm1b,

CGGAATTCATGGCGGGTCCGCAAAATGGG and
GCTCTAGAACTCAGTTTTTGCAGGAGTT,

For RIP3,

TGCTGGAAGAGAAGTTGAGTTGC and
CTGTTGCACACTGCTTCGTACAC. Anti-RIP3 antibody was purchased from SantaCruz.

Metabolites extraction

Cells were washed twice with ice-cold phosphate-buffered saline (PBS, pH 7.4) to move medium components and collected with a cell lifter in 1ml -80°C methanol gently and quickly on ice. Then cells were centrifuged at 1000 g for 5 min (at 4°C) to collect pellet and supernatant separately. Immediately cell pellet was flash frozen in liquid N₂ to maintain their biochemical integrity. After the pellet was lyophilized, dry weight of cells was recorded for normalizing metabolite contents. The supernatant was also lyophilized to reduce the loss of cellular metabolites. The lyophilized powders (5-10 mg) were extracted in eppendorf tubes with 40-60:1 (v/w) volumes with ice-cold 10% (w/v) ice-cold trichloroacetic acid (TCA). The mixture was homogenized by liquid N₂ grinding method on ice. Then homogenate was centrifuged at ≥ 15,000 rpm for 30 min (at 4°C) twice to collect supernatant. The pooled TCA extract could be lyophilized to remove TCA for further research²³.

NMR

The dried material was dissolved in 50 µL D₂O, incubated for 2 h at room temperature, centrifuged to remove particulates and loaded into NMR tubes. For identifying metabolites and determining the positional enrichment with ¹³C we used 2D experiments including HSQC and TOCSY, comparing with the standards library from Fan et al ²⁴. Metabolites were identified on the basis of 1H and 13C chemical shifts, and TOCSY connectivity pattern.

¹H- ¹³C HSQC (heteronuclear single quantum coherence spectroscopy) was performed as described by Szyperski²⁵, performed at 21°C and a ¹³C resonance frequency of 125 MHz using a Bruker AV500 spectrometer. ¹H TOCSY (total correlation spectroscopy) was recorded in the same spectrometer with a spectral width of 6000 Hz in F2, 0.341 s acquisition time in t2 and 0.05 s in t1, 1.9 s interpulse delay, 50 ms mixing time, and an 8 kHz B1 field strength ²⁶. In this study, the integration volume generated by SPARKY was adopted as the intensity of each peak.

GC-MS

Following NMR analysis, 5µL aliquot was lyophilized to remove heavy water. The dried material was silylated with 100 µL of tetrahydrofuran (Fluka), 100 µL of N- (tert-butyldimethylsilyl)-N-methyl-trifluoroacetamide (MTBSTFA) (Fluka), and the mixture was incubated for 60 min at 60°C. Treatment of amino acids with MTBSTFA yields the corresponding tert-butyldimethylsilyl (TBDMS) derivatives that have good characteristics for GC-MS measurement²⁷. GC-MS experiments were performed using a Thermo Finnigen Trace gas chromatograph quadrupole mass selective detector (electron impact ionization), operated at 70 eV, equipped with an autosampler/injector (Agilent Technologies, Palo Alto, CA). The column DB-5 device (JR Scientific, Woodland, CA)

was used for analysis by applying the parameters reported by previous works²⁷.

Metabolites were identified by matching against Agilent NIST libraries on the basis of GC retention times and mass fragmentation patterns. The identification were all verified by manual inspection. GC-MS quantification of total abundance of metabolites was accomplished by comparing the m/z 147 ion response for each metabolite in the samples with that for the corresponding standard of known concentration.

RT-PCR Studies

HeLa cells were harvested with 0.05% trypsin for mRNA expression analyses. Total RNA was isolated with cold Trizol and isopropanol. The cDNAs were synthesized with the Prime-Script™1st Strand cDNA synthesis kit (Takara) according with the manufacturer's instructions and stored at -40°C prior to use. Real-time PCR (RT-PCR) was carried out on the Applied Biosystems 7000 real-time PCR system (Applied Biosystems) using SYBR Premix ExTaq™ (TaKaRa). Primers used for RT-PCR were as follows:

For RIP1, AGTCCTGGTTGCTCCTTCCC and
CGGTCTCCTTTCCTCTCTCTG

For PYGL, CTAAGAAGTTATTCGTGCCA and
CTTCATATTGCTGTCCC

For ACT,CTATCCCAGTGTCTATCCA and
TGCTCCACAGCAAACCC

For LDH, AGCAAGAGGGAGAAAGCC and
TCCAAGCCACGTAGGTCA

For PDH, CCTTCAGCCTGTGCCTAT and
CACCACCACTGGATTGTTA

For GLUD1, CACCTCAGCAAGTTCCCCT and
GAGCCATCGAAATTCCTC

For GLUL, ATGACCACCTCAGCAAGTT and
CAGCAGGCACGAGATACA

For ACL, ACGGATGGCGTCTATGAG and
CTGGTTCTTGCTACTGC

All measurements were performed in triplicate.

Enzyme activity assays

To prepare cell extract for enzyme activity, about 1×10^7 cells were harvested by trypsinization and washed twice with cold PBS. Then cells were suspended in 500µl of lysis buffer (20 mM Tris-HCl pH 7.5, 150 mM NaCl, 1% Triton X-100, 2 mM EDTA, 1 mM β-Glycerophosphate, 1 mM Na₃VO₄, 1 mM PMSF, and protease inhibitors) and lysed for 20 min. After sonication for 20 second on ice, cell lysates were centrifuged at 13,000 rpm for 10 min at 4 °C. The debris was removed and the supernatant was used for

determination of enzyme activities²¹. Each experiment was repeated three times. Enzyme activities were measured spectrophotometrically in a thermostatically controlled recording spectrophotometer (Beckman DU50).

For PYGL, the enzyme activity was measured based on the manufacturer's instructions of a Cell GP Assay kit (GenMed Scientifics Inc., Shanghai, China). The cell lysates were added to reaction buffer containing glycogen, phosphoglucomutase, and glucose-6-phosphate dehydrogenase, and NADP at 37 °C for 2 minutes. NADPH production was monitored at 340 nm for 5 minutes at 37°C. For GLUL, the cell lysates were added to 800 µL of GLUL assay buffer, containing 120 mM L-glutamine, 10 mM sodium arsenate, 50 mM imidazole, 30 mM hydroxylamine, 30 µM MnCl₂, and 200 µM ATP, pH 6.5, and incubated 60 min at 37°C. The stop solution includes FeCl₃·7H₂O (15%, w/v), trichloroacetic acid (25%, v/v), and HCl (2.5 M). The absorbencies of samples were measured at 540 nm. For GLUD1, The cell lysates were added to reaction buffer containing 50 mM triethanolamine buffer (pH 8.0), 100 mM ammonium acetate, 150 µM NADPH, 2.6 mM EDTA, and 1 mM ADP. 8 mM α-ketoglutarate was added to the mixture to start reaction. The decrease in absorbance at 340 nm was monitored for 5 minutes. The PYGL, GLUL and GLUD1 activities were assayed based on earlier studies²¹. For PDH, 1ml reaction system contains 50 mmol Potassium phosphate buffer, pH 7.4, 1.0 mmol MgCl₂, 0.05 mmol CoAS-Na, 3.0 mmol Cys-HCl, 0.2 mmol TPP, 2.0 mmol β-NAD, 2.0 mmol sodium pyruvate and cell lysis buffer, NADH production was monitored at 340nm for 10min at 37°C.

Statistical Analysis

Values are shown as mean ± standard deviation (SD) or standard error of the mean (SEM). Data were analyzed using the two-tailed t-test, and significance was defined as $p < 0.05$.

FIGURE LEGENDS

Figure 1. Growth of HeLa cells transfected with JHDM1B shRNA was inhibited.

(A) mRNA levels of Jhdm1b from HeLa cells transfected empty vector and Jhdm1b shRNA determined by quantitative real-time PCR (qRT-PCR). All data were normalized against levels of actin. (B) Proliferation of HeLa cells transfected with Jhdm1b and control siRNA. The error bars represent SEM. (n=3)

Figure 2. Pentose phosphate pathway was not activated by Jhdm1b knockdown.

(A) The proportion of [2,3-¹³C] to [2-¹³C] lactate in wild type and Jhdm1b knockdown cells, calculated with intensities of cross peaks in HSQC spectra. (B) The proportion of m+1 to m+2 isotopologues of lactate in wild type and Jhdm1b knockdown cells, calculated from intensities of isotopologues in GC-MS spectra. 1,2-¹³C glucose was used as carbon source in medium. The error bars represent SEM. (n=3)

Figure 3. Jhdm1b knockdown upregulated RIP3 expression.

(A) RIP3 and RIP1 expression in wild type and Jhdm1b knockdown cells determined by qRT-PCR. The error bars represent SEM. (n=3)

(B) RIP3 and RIP1 expression in wild type and Jhdm1b knockdown cells determined by Western blotting with antibody to RIP3.

Figure 4. Comparison of expression level and activity of some metabolic enzymes.

(A) qRT-PCR was employed to determine the expression level of seven metabolic enzymes including LDH, PDH, ACL, ACT, GLUD1, PYGL and GLUL. (B) Activities of PDH and Rip3-related enzymes were determined by spectrometry. The error bars represent SEM, (n=3) *P<0.05 by a two-tailed t-test.

Figure 5. Expression level and activity of metabolic enzymes recover partly in RIP3/Jhdm1b double knockdown cells.

The expression levels (A) and activities (B) of PDH and RIP3-related metabolic enzymes in wild type, Jhdm1b knockdown and Jhdm1b/RIP3 double knockdown HeLa cells were determined by qRT-PCR and spectrometry. The error bars represent SEM, (n=3) *P<0.05 by a two-tailed t-test.

Acknowledgements

We thank Professor Mian Wu & Yide Mei (School of Life Science, University of Science and Technology of China) for providing cell lines and technical support on RNAi. We also thank Dr. Bo Wu (Hefei Institutes of Physical Science, Chinese Academy of Sciences) for helping guide the NMR experiment.

ARTICLE

Notes and references

This work was financially supported by the National Basic Research Program of China (973 Program, grants 2011CB966302, 2012CB917201 and 2011CB911104); the Chinese National Natural Science Foundation (grant 31170693, 31330018); Research Program of the Chinese Academy of Sciences (Grant No. KJZD-EW-L05); The Strategic Priority Research Program of the Chinese Academy of Sciences, Grant No. XDB08010101.

The abbreviations used are: SIRM, stable isotope resolved metabolomics; RIP3, Receptor interacting protein 3; KMTs, lysine methyltransferases; KDMs, lysine demethylases; SAM, S-adenosyl methionine;

FAD, flavin adenine dinucleotide; JhdM, JmjC-domain-containing histone demethylase;

PRC, Polycomb Repressive Complex; ROS, reactive oxygen species; MEF, mouse embryo fibroblast; Crabp2, Cellular retinoic acid-binding protein II; PYGL, glycogen phosphorylase;

GLUL, glutamate-ammonia ligase; GLUD1, glutamate dehydrogenase 1; GC-MS, gas chromatography-mass spectroscopy; NMR, Nuclear magnetic resonance; BSA, bovine serum albumin; PBS, phosphate-buffered saline;

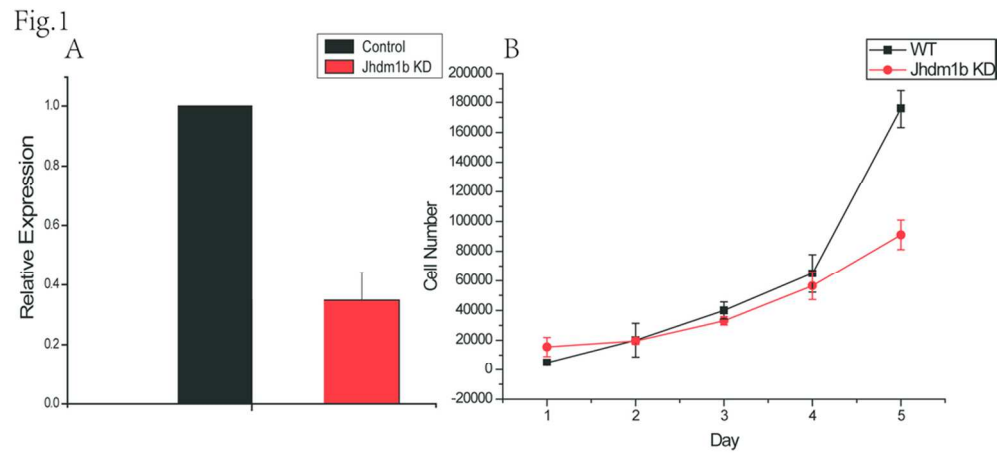
TCA, trichloroacetic acid; HSQC, heteronuclear single quantum coherence spectroscopy; TOCSY, total correlation spectroscopy; MTBSTFA, N-(tert-butyl)dimethylsilyl)-N-methyl-trifluoroacetamide; TBDMS, tert-butyl dimethylsilyl; GSH, Glutathione; RA, retinoic acid; ROS, Reactive Oxygen Species; PDK, pyruvate dehydrogenase kinases; PDP, pyruvate dehydrogenase phosphatases; α -KG, α -ketoglutarate; PP pathway, pentose phosphate pathway; ACT, Aspartate carbamyl transferase; PC, pyruvate

carboxylation. AcCoA, acetyl coenzyme A; PDH, Pyruvate dehydrogenase; LDH, lactate dehydrogenase.

1. B. Campos, R. Warta, J. Chaisaingmongkol, L. Geiselhart, O. Popanda, C. Hartmann, A. von Deimling, A. Unterberg, C. Plass, P. Schmezer and C. Herold-Mende, *International Journal of Cancer*, 131, 1963-1968.
2. F. Weinberg, R. Hamanaka, W. W. Wheaton, S. Weinberg, J. Joseph, M. Lopez, B. Kalyanaraman, G. M. Mutlu, G. R. S. Budinger and N. S. Chandel, *Proceedings of the National Academy of Sciences*, 107, 8788-8793.
3. T. W. Fan, M. Kucia, K. Jankowski, R. M. Higashi, J. Ratajczak, M. Z. Ratajczak and A. N. Lane, *Molecular cancer*, 2008, 7, 79.
4. S. Matoba, J.-G. Kang, W. D. Patino, A. Wragg, M. Boehm, O. Gavrilova, P. J. Hurley, F. Bunz and P. M. Hwang, *Science*, 2006, 312, 1650-1653.
5. P. Gao, I. Tchernyshyov, T. C. Chang, Y. S. Lee, K. Kita, T. Ochi, K. I. Zeller, A. M. De Marzo, J. E. Van Eyk, J. T. Mendell and C. V. Dang, *Nature*, 2009, 458, 762-765.
6. J. C. Black and J. R. Whetstone, *Biopolymers*, 2013, 99, 127-135.
7. H. J. Wang, Y. J. Hsieh, W. C. Cheng, C. P. Lin, Y. S. Lin, S. F. Yang, C. C. Chen, Y. Izumiya, J. S. Yu, H. J. Kung and W. C. Wang, *Proceedings of the National Academy of Sciences of the United States of America*, 2014, 111, 279-284.
8. F. Kottakis, P. Fotopoulou, I. Sanidas, P. Keller, A. Wronski, B. T. Dake, S. A. Ezell, Z. Shen, S. P. Naber, P. W. Hinds, E. McNeil, C. Kuperwasser and P. N. Tschlis, *Cancer research*, 2014, DOI: 10.1158/0008-5472.CAN-13-2733.
9. J. He, E. M. Kallin, Y. Tsukada and Y. Zhang, *Nature structural & molecular biology*, 2008, 15, 1169-1175.
10. A. Janzer, K. Stamm, A. Becker, A. Zimmer, R. Buettner and J. Kirfel, *The Journal of biological chemistry*, 2012, 287, 30984-30992.
11. D. Wiederschain, W. Susan, L. Chen, A. Loo, G. Yang, A. Huang, Y. Chen, G. Caponigro, Y.-m. Yao, C. Lengauer, W. R. Sellers and J. D. Benson, *Cell Cycle*, 2009, 8, 498-504.
12. A. Le, A. N. Lane, M. Hamaker, S. Bose, A. Gouw, J. Barbi, T. Tsukamoto, C. J. Rojas, B. S. Slusher, H. Zhang, L. J. Zimmerman, D. C. Liebler, R. J. Slebos, P. K. Lorkiewicz, R. M. Higashi, T. W. Fan and C. V. Dang, *Cell metabolism*, 2012, 15, 110-121.
13. C. M. Metallo, P. A. Gameiro, E. L. Bell, K. R. Mattaini, J. Yang, K. Hiller, C. M. Jewell, Z. R. Johnson, D. J. Irvine, L. Guarente, J. K. Kelleher, M. G. Vander Heiden, O. Iliopoulos and G. Stephanopoulos, *Nature*, 2012, 481, 380-384.
14. C. Polytarhou, R. Pfau, M. Hatziaepostolou and P. N. Tschlis, *Mol Cell Biol*, 2008, 28, 7451-7464.

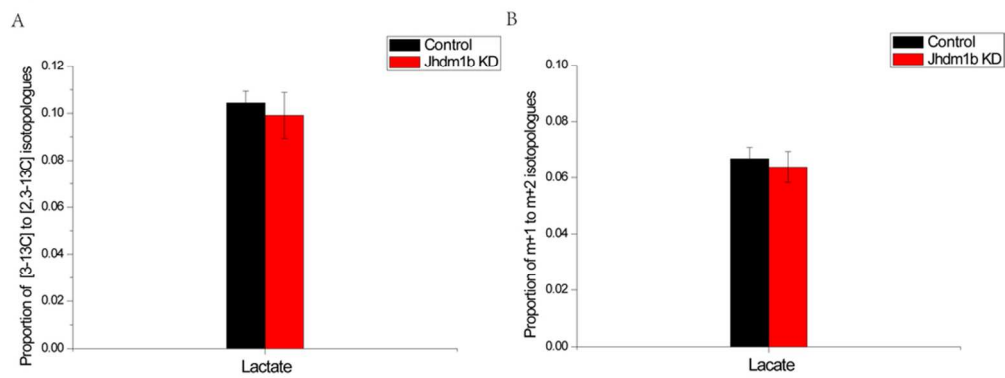
ARTICLE

15. B. L. Bartnik, S. M. Lee, D. A. Hovda and R. L. Sutton, *Journal of neurotrauma*, 2007, 24, 1079-1092.
16. R. Teperino, K. Schoonjans and J. Auwerx, *Cell metabolism*, 2010, 12, 321-327.
17. A. Tzatsos, P. Paskaleva, S. Lymperi, G. Contino, S. Stoykova, Z. Chen, K. K. Wong and N. Bardeesy, *The Journal of biological chemistry*, 2011, 286, 33061-33069.
18. A. Imbard, A. Boutron, C. Vequaud, M. Zater, P. de Lonlay, H. O. de Baulny, C. Barnerias, M. Mine, C. Marsac, J. M. Saudubray and M. Brivet, *Molecular genetics and metabolism*, 2011, 104, 507-516.
19. K. P. Patel, T. W. O'Brien, S. H. Subramony, J. Shuster and P. W. Stacpoole, *Molecular genetics and metabolism*, 2012, 105, 34-43.
20. L. R. Gray, S. C. Tompkins and E. B. Taylor, *Cellular and molecular life sciences : CMLS*, 2014, 71, 2577-2604.
21. D.-W. Zhang, J. Shao, J. Lin, N. Zhang, S.-C. Lin and J. Han, *Science*, 2009, 325.
22. J. M. Thornburg, K. K. Nelson, B. F. Clem, A. N. Lane, S. Arumugam, A. Simmons, J. W. Eaton, S. Telang and J. Chesney, *Breast cancer research : BCR*, 2008, 10, R84.
23. T. W. M. Fan, R. M. Higashi and A. N. Lane, *Drug Metabolism Reviews*, 2006, 38, 707 - 732.
24. T. W.-M. Fan, *Progress in Nuclear Magnetic Resonance Spectroscopy*, 1996, 28, 161-219.
25. T. Szyperski, *European Journal of Biochemistry*, 1995, 232, 433-448.
26. T. Fan, L. Bandura, R. Higashi and A. Lane, *Metabolomics*, 2005, 1, 1 - 15.
27. B. Rui, T. Shen, H. Zhou, J. Liu, J. Chen, X. Pan, H. Liu, J. Wu, H. Zheng and Y. Shi, *BMC systems biology*, 2010, 4, 122.



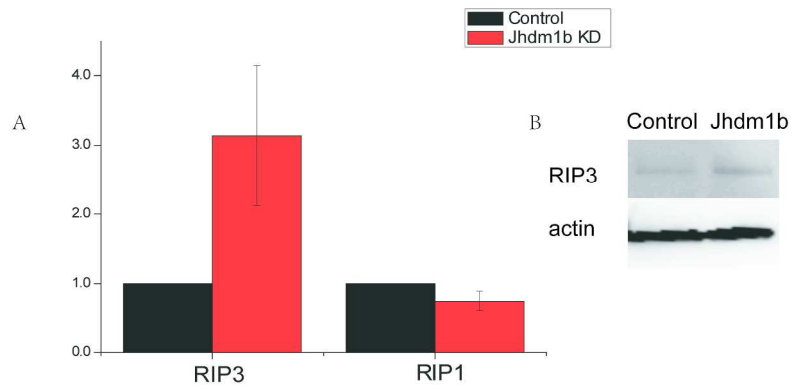
94x42mm (300 x 300 DPI)

Fig.2



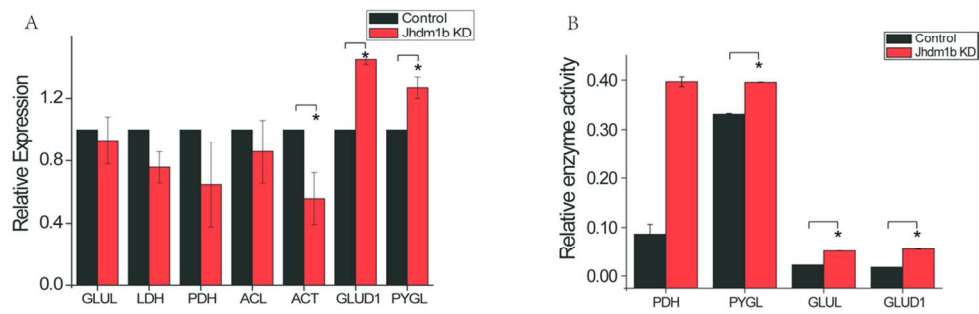
86x35mm (300 x 300 DPI)

Fig.3



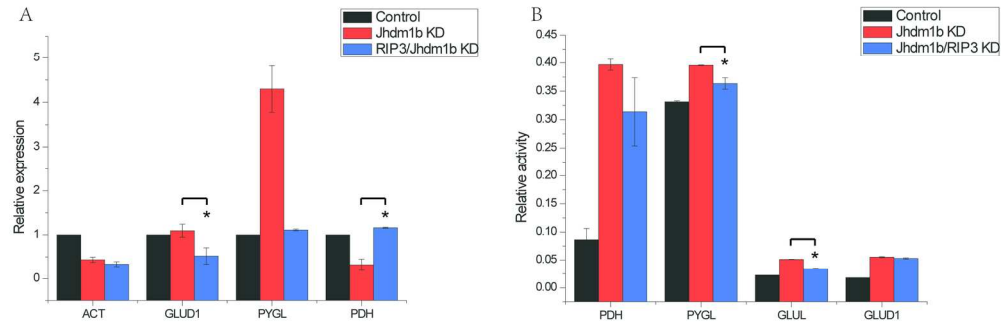
229x327mm (300 x 300 DPI)

Fig.4



106x56mm (300 x 300 DPI)

Fig.5



169x144mm (300 x 300 DPI)